



**PAPER****OPEN ACCESS**RECEIVED
4 August 2023REVISED
23 October 2023ACCEPTED FOR PUBLICATION
6 November 2023PUBLISHED
17 November 2023Original content from
this work may be used
under the terms of the
[Creative Commons
Attribution 4.0 licence](#).Any further distribution
of this work must
maintain attribution to
the author(s) and the title
of the work, journal
citation and DOI.

Tuning quantum pathway interference in two-color laser photoemission using DC bias

Yang Zhou^{1,2}  and Peng Zhang^{1,*} ¹ Department of Electrical and Computer Engineering, Michigan State University, East Lansing, MI 48824, United States of America² Argonne National Laboratory, Lemont, IL 60439, United States of America

* Author to whom any correspondence should be addressed.

E-mail: pz@egr.msu.edu**Keywords:** photoemission, two-color laser, DC bias, quantum pathway interference**Abstract**

Coherent control of quantum systems depends on the manipulation of quantum interference through external fields. In this work, we investigate the effects of DC bias field on coherent control of quantum pathways in two-color laser photoemission using exact analytical solutions of the one-dimensional time dependent Schrödinger equation. Increasing DC bias lowers and narrows the surface potential barrier, shifting the dominant emission to lower order multiphoton photoemission, photo-assisted tunneling and then direct tunneling. Those lower order photon absorption processes result in fewer possible pathways, and therefore modulation of photoemission current can be suppressed as DC field increases. It is shown that a maximum modulation depth of 99.4% can be achieved for a gold emitter at local DC bias $F_0 = 0.5 \text{ V nm}^{-1}$, fundamental (800 nm) laser field $F_1 = 2.6 \text{ V nm}^{-1}$ and second harmonic laser field $F_2 = 0.25 \text{ V nm}^{-1}$. For a given set of input parameters, the total photoemission consists of different k -photon processes, each of which has their own different multiple possible pathways and interference effects. However, the quantum pathways and their interference for the dominant k -photon process and for the total photoemission probability show the same trends. This study demonstrates strong flexibility in tuning two-color lasers induced photoemission using a DC bias and provides insights into coherent control schemes of general quantum systems.

1. Introduction

Quantum interference manipulation via external fields is fundamental to coherent control of quantum systems. Two-color laser fields, containing a strong fundamental (ω) and a weaker second harmonic (2ω), provide a powerful tool for probing and manipulating electron dynamics in nanostructures with nanometer spatial and ultrashort temporal resolutions [1–5], which makes it useful in a wide range of applications, including high-harmonic generation [6, 7], surface plasmon measurement and characterization [8–10], and opto- or lightwave- electronics [11–17]. The strongly modulated electron sources triggered by the mixed laser fields play an important role in time-resolved transmission microscopy [18–23], compact x-ray sources [24–26], and free-electron lasers [27]. Multiple electron emission mechanisms, i.e. multiphoton photoemission, above-threshold photoemission and optical field emission, depending on the laser intensities and wavelengths, have been demonstrated experimentally and theoretically [3, 28–32]. By sweeping the relative phase and controlling the intensity ratio between the fundamental and its second harmonic laser fields, photoemission current can be enhanced or suppressed (relative to photoemission by a single color laser), with a modulation depth of up to 97.5% observed in experiments [3, 33–36]. The modulation depth (also termed as visibility) is defined as the ratio of the difference between maximum and minimum of photoemission current and the sum of them. The high modulation depth is ascribed to the interference among competing pathways. In addition to single-color pathways (absorption of ω photons only or 2ω photons only), the mixture of two-color lasers also introduces multicolor pathways (simultaneous absorption

of both ω photon(s) and 2ω photon(s)). Quantum pathways interference model has been used to explain the scaling of the coherent signal to the second-harmonic laser intensity in experiments [3, 31, 33, 36].

A DC bias field can offer additional tunability for the coherent control over electron dynamics [15, 30, 37–39]. Due to the lowering and narrowing of the surface potential barrier by the DC field, lower order photon absorption channels are opened, and therefore electron emission can be enhanced from a few times to orders of magnitudes, depending on the magnitude of DC field, laser fields and laser wavelengths [33, 40, 41]. It has been shown that DC field has stronger influence in longer laser wavelength range or higher order of multiphoton absorption regime [32, 42]. A decreased modulation depth with increasing DC bias field has been observed in photoemission by two-color lasers [31, 33]. Systematic analysis of quantum pathways interference using exact quantum model reveals the effects of two-color lasers and DC field on the coherent modulation of photoemission [43]. It is found that increasing the intensity ratio of the second harmonic to fundamental lasers results in stronger pathways interference and increased modulation depth. Increasing DC bias sequentially suppresses higher frequency terms, leading to two peaks in the modulation depth vs DC field. While it is known that a static field shifts the dominant emission processes to lower order photon emission [30, 40], our previous work [43] and other previous experimental analyses [31, 33] on quantum pathways were restricted to multiphoton absorption with the order $k_0 = \langle W_0/\hbar\omega \rangle + 1$, where $\langle \rangle$ denotes the integer part inside the bracket, with W_0 being the nominal work function of the cathode, and $\hbar\omega$ the photon energy of the fundamental laser. Thus, how DC bias shifts multiphoton processes to a different photon order and therefore influences the possible pathways and the weight of each pathway and interference among them cannot be revealed through existing analysis and needs further study.

In this work, we analyze the effects of DC field on two-color laser photoemission using quantum pathways interference with the exact analytical solutions of the time-dependent Schrödinger equation (TDSE). Our analysis explicitly shows how DC bias shifts the possible pathways, changes the weight of each pathway and interference among them, and modulates photoemission current.

2. Quantum pathways interference

The one-dimensional model is illustrated in figures 1(a)–(e) for photoemission under various combinations of DC bias field F_0 and two-color laser field $f(t) = F_1 \cos\omega t + F_2 \cos(2\omega t + \theta)$, where F_1 and F_2 are the magnitudes of the fundamental and second harmonic laser fields respectively, ω is the angular frequency of the fundamental laser, θ is the relative phase between the two laser fields. All fields are assumed to be perpendicular to the metal surface and abruptly cut off inside the metal ($x < 0$). Electrons with initial energy of ε emit through the metal-vacuum interface ($x = 0$). The potential barrier relative to the bottom of the energy band reads,

$$\phi(x, t) = \begin{cases} 0, & x < 0 \\ E_F + W_{\text{eff}} - ef(t)x - eF_0x, & x \geq 0 \end{cases} \quad (1)$$

where E_F is the Fermi energy of the metal, and $W_{\text{eff}} = W_0 - W_{\text{Schottky}}$ is the effective work function with W_0 the nominal work function of the metal and $W_{\text{Schottky}} = 2(e^3 F_0/16\pi\varepsilon_0)^{1/2}$ the Schottky barrier lowering due to F_0 , e (>0) is the elementary charge, and ε_0 is the vacuum permittivity. By exactly solving TDSE subject to the potential barrier in equation (1), the time-averaged electron transmission probability from energy level ε is [29, 30]

$$D(\varepsilon) = \sum_{k=-\infty}^{\infty} w_k(\varepsilon), \quad (2)$$

where $w_k(\varepsilon)$ represents the electron emission through k -photon ($\hbar\omega$) processes, with $k < 0$ being multiphoton emission, $k = 0$ direct tunneling, and $k > 0$ multiphoton absorption processes. Each k -photon ($\hbar\omega$) process also includes the possible processes of substituting two fundamental photons $2\hbar\omega$ with a single second-harmonic photon $\hbar(2\omega)$, as illustrated in figures 1(a)–(c). Time-dependent electron transmission probability can display more electron dynamics under dichromatic lasers and DC bias. Detailed derivations are provided in [29] and [30]. An example of time- and space- dependent transmission probabilities can be found in figure 5 in [29]. We would like to point out that the lasers in the model are assumed to be continuous waves (CW). Good agreements of our model using CW lasers with both experiments [30] and simulations [40] for laser pulses with a duration >10 optical cycles have been demonstrated. The model based on CW lasers [30] also reproduces the energy spectrum of different n -photon excited states (figure 10(a) in [30]) as well as the modulation profile in the experiment (figure 10(b) in [30]).

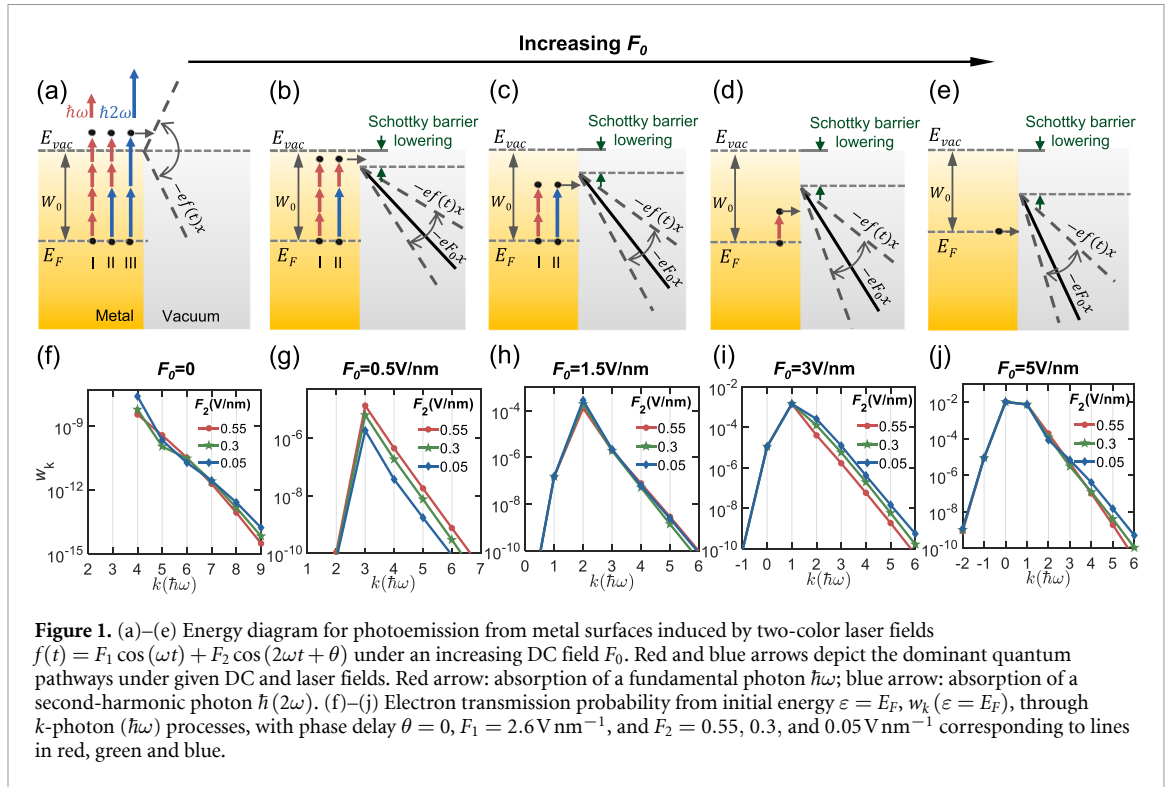


Figure 1. (a)–(e) Energy diagram for photoemission from metal surfaces induced by two-color laser fields $f(t) = F_1 \cos(\omega t) + F_2 \cos(2\omega t + \theta)$ under an increasing DC field F_0 . Red and blue arrows depict the dominant quantum pathways under given DC and laser fields. Red arrow: absorption of a fundamental photon $\hbar\omega$; blue arrow: absorption of a second-harmonic photon $\hbar(2\omega)$. (f)–(j) Electron transmission probability from initial energy $\varepsilon = E_F$, $w_k(\varepsilon = E_F)$, through k -photon ($\hbar\omega$) processes, with phase delay $\theta = 0$, $F_1 = 2.6 \text{ V nm}^{-1}$, and $F_2 = 0.55, 0.3, \text{ and } 0.05 \text{ V nm}^{-1}$ corresponding to lines in red, green and blue.

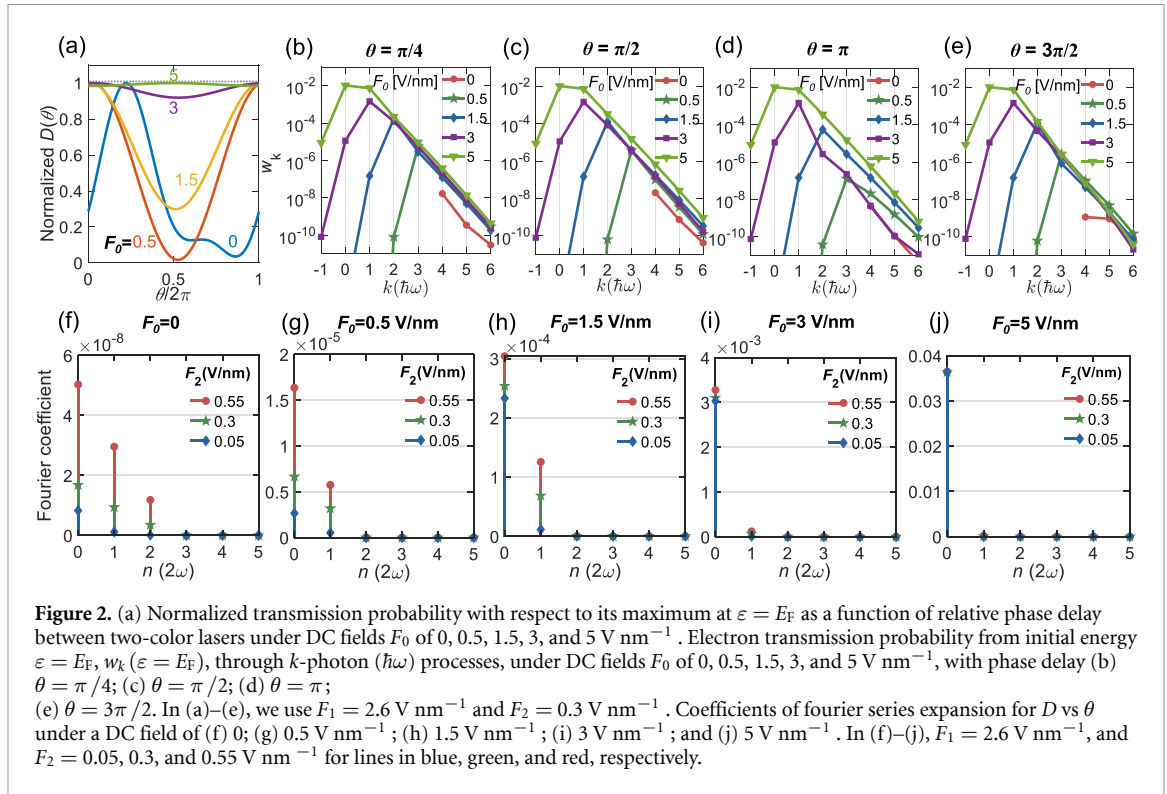
Figures 1(f)–(j) show the electron emission probability from Fermi level $w_k(\varepsilon = E_F)$ through k -photon ($\hbar\omega$) processes under a DC field of 0, 0.5, 1.5, 3, and 5 V nm^{-1} , respectively, with the fundamental laser field $F_1 = 2.6 \text{ V nm}^{-1}$, the second harmonic laser field $F_2 = 0.55, 0.3, 0.05 \text{ V nm}^{-1}$ corresponding to lines in red, green and blue, and the relative phase $\theta = 0$. The metal is assumed to be gold, with $W_0 = 5.1 \text{ eV}$ and $E_F = 5.53 \text{ eV}$. The fundamental laser has a wavelength of 800 nm ($\hbar\omega = 1.55 \text{ eV}$), and the dominant emission process is equivalent 4 $\hbar\omega$ -photon absorption when $F_0 = 0$, as shown in figure 1(f). Increasing the applied DC field shifts the dominant k -photon process to lower order multiphoton absorption photoemission ($k < 4$, figures 1(b) and (g)), photo-assisted tunneling (figures 1(c), (h) and (d), (i)) or direct tunneling (figures 1(e) and (j)) [32, 41, 42], resulting in different dominant photon absorption pathways. Tunneling effect under DC bias (figures 1(c)–(e)) lowers the number of required photons for multiphoton photoemission and decreases the number of possible pathways. The interference effect among pathways becomes weaker and photoemission is therefore less modulated. The possible multiphoton absorption pathways include single color photon absorption pathways, e.g. pathways I and III in figure 1(a), and multicolor pathways, e.g. pathway II in figure 1(a). According to the power scaling law between photoemission current and laser intensity with laser heating effects ignored [40, 42, 44], the total transmission probability D in equation (2) can be written as a power function of second harmonic laser intensity ($\sim F_2^2$),

$$D_i = K_i (F_2^2)^{(k-s)/2}, \quad (3)$$

where i represents i th pathway in figures 1(a)–(d), k is the number of total equivalent $\hbar\omega$ photons (as in equation (2)), s is the number of absorbed $\hbar\omega$ photons, $(k-s)/2 = 0, 1, 2, \dots$ is an integer representing the number of absorbed $\hbar(2\omega)$ photons. Implied by equation (3) is that the power scaling relationship between transmission probability and fundamental laser intensity is incorporated in K_i [43]. Interference occurs among different pathways, resulting in coherent modulation of photoemission current with higher frequencies. Take $F_0 = 0.5 \text{ V nm}^{-1}$ as an example (figure 1(b)), with pathway I: absorption of 3 $\hbar\omega$ photons and pathway II: absorption of 1 $\hbar\omega$ photon and 1 $\hbar(2\omega)$ photon. The interference between them is,

$$D_{\text{I\&II}} = K_{\text{I\&II}} \sqrt{F_2^2} \cos\theta. \quad (4)$$

which has a frequency of 2ω indicated by the phase delay θ between the two lasers. A maximum DC bias field of 5 V nm^{-1} has been considered here, which is below the threshold breakdown DC field (after local field enhancement) for sharp tips made of common emitter materials [30, 45]. Nanotips survive large fields better for short pulse durations. A local DC electric field of up to 10 V nm^{-1} can be realized in experiments on



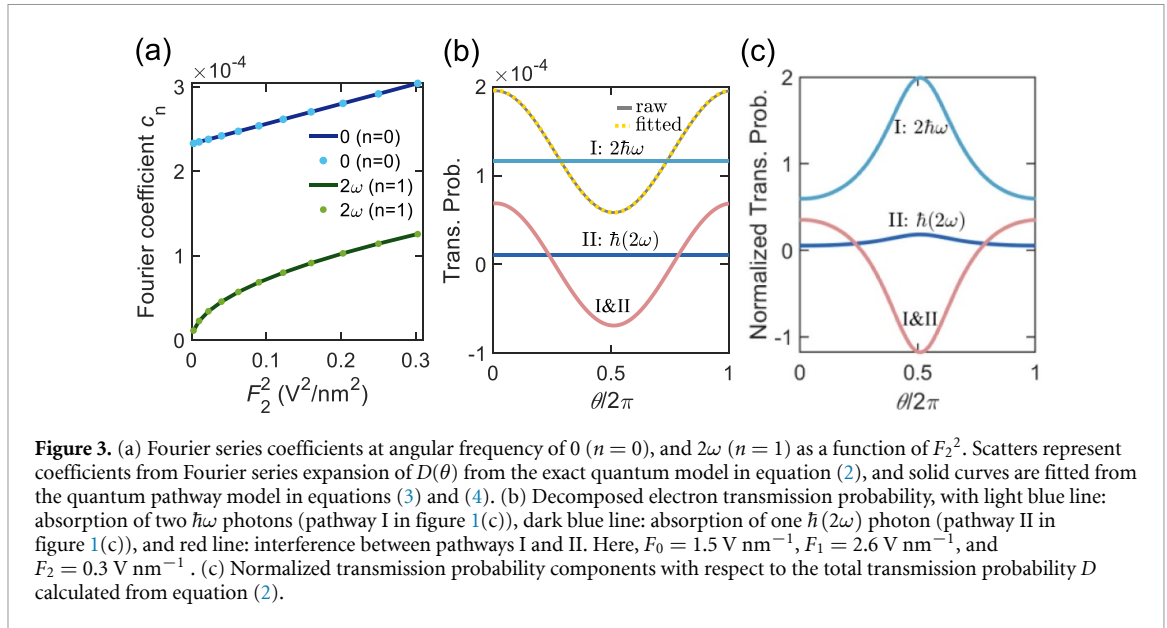
nanostructures (after field enhancement), through laboratory-scale setup based on pulsed capacitor discharge [45, 46] or powerful THz pulses [37, 47].

Figure 2(a) shows the normalized transmission probability with respect to the maximum D in each case for 2π period of θ under different DC field F_0 . It is observed that the location of the minimum of D shifts from $\theta \approx 1.7\pi$ to $\theta \approx \pi$ as F_0 increases. The modulation depth becomes smaller, as shown by the minimum D shifting from being close to 0 for $F_0 = 0$ and 0.5 V nm^{-1} to being around 1 for a stronger DC field of $F_0 = 5 \text{ V nm}^{-1}$. Electron emission energy spectra under different relative phase delay in figures 2(b)–(e) show that the dominant photoemission channel shifts from $k = 4$ to 0 as DC field increases from 0 to 5 V nm^{-1} , which is consistent with figures 1(f)–(j). As DC field increases, the electron emission energy spectrum (specifically its peak) becomes less sensitive to the phase delay θ .

The periodic transmission probability D vs phase delay θ can be expanded in terms of Fourier series, resulting in terms at multiples of second harmonic frequency 2ω ,

$$D(\tau) = \frac{c_0}{2} + \sum_{n=1}^N c_n \sin(n(2\omega)\tau + \varphi_n) \quad (5)$$

where $\tau = \theta/2\omega$ is phase delay time, $c_0 = \frac{2}{T} \int_0^T D(\tau) d\tau$, $c_n = \sqrt{a_n^2 + b_n^2}$, $a_n = \frac{2}{T} \int_0^T D(\tau) \cos(n(2\omega)\tau) d\tau$, $b_n = \frac{2}{T} \int_0^T D(\tau) \sin(n(2\omega)\tau) d\tau$, $T = \frac{2\pi}{2\omega}$, and $\varphi_n = \tan^{-1}\left(\frac{a_n}{b_n}\right)$. Figures 2(f)–(j) show the Fourier series coefficients for $D(\varepsilon = E_F)$ vs θ at multiples of second-harmonic laser frequency 2ω . When $F_0 = 0$, three dominant components at 0, 2ω , 4ω are observed. As seen in [43], increasing the intensity ratio of the second harmonic to fundamental lasers results in relative less contribution from the ω pathway (I in figure 1(a)), more contribution from multicolor pathway (absorption of both ω and 2ω photons, II in figure 1(a)) and 2ω pathway (III in figure 1(a)), and stronger interference effects between pathways II and III. As F_0 increases, the high frequency terms at 4ω and 2ω are suppressed sequentially, which is consistent with the observation that the dominant channel shifts towards lower order multiphoton photoemission, photo-assisted tunneling, and direct tunneling. When $F_0 = 0.5$ and 1.5 V nm^{-1} , two dominant components at 0 and 2ω frequencies are observed (figures 2(g) and (h)). There are two possible pathways observed, with the single fundamental photon absorption pathway and multicolor pathway including one $\hbar\omega$ and one $\hbar(2\omega)$ in figure 1(b), and single fundamental photon pathway and single second harmonic photon pathway in figure 1(c). The 2ω frequency term comes from the interference between those two pathways. When $F_0 = 3$ and 5 V nm^{-1} , only dominant DC terms in the Fourier analysis can be observed. As shown in figures 1(i) and (j), the dominant



photoemission channel is $k = 1$ and 0 respectively. No extra photon absorption pathway is possible for the dominant emission processes (figures 1(d) and (e)) and therefore there are no interference effects in these cases and the coherent modulation of photoemission current is suppressed.

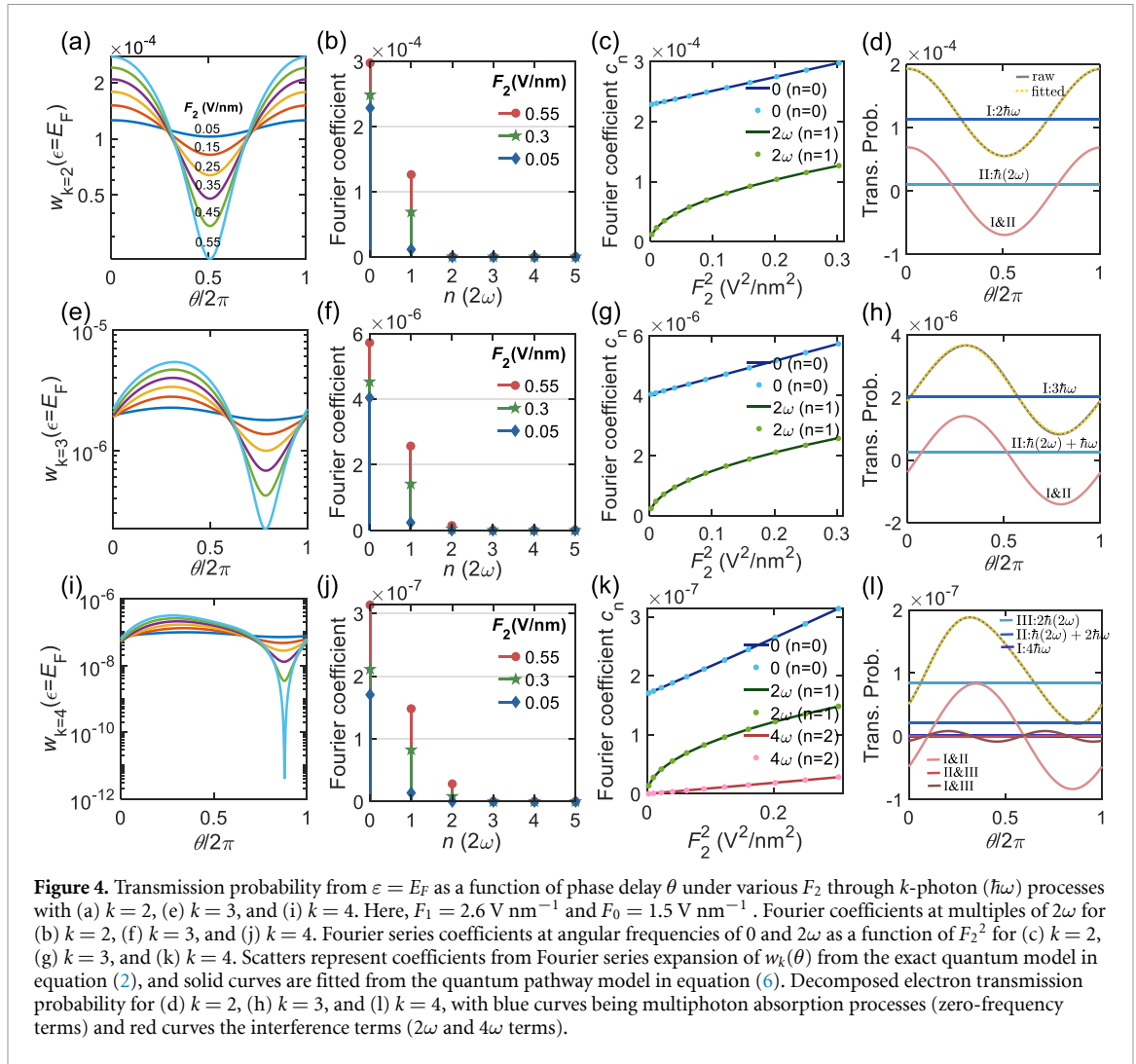
Fourier series coefficients of transmission probability vs θ under different F_2 can be fitted with the quantum pathways interference model, i.e. equations (3) and (4). Therefore, the prefactor K_i can be obtained and electron emission through each possible pathway and interference among them can be explicitly identified [43]. Figure 3(a) shows Fourier series coefficients at various 2ω laser intensities, with scatters obtained from Fourier series expansion and solids lines being the fitting results. Here, $F_1 = 2.6 \text{ V nm}^{-1}$ and $F_0 = 1.5 \text{ V nm}^{-1}$. The fitted prefactors are $K_I = 1.16 \times 10^{-4}$, $K_{II} = 1.16 \times 10^{-4} (\text{V nm}^{-1})^{-2}$, and $K_{I\&II} = 2.29 \times 10^{-4} (\text{V nm}^{-1})^{-1}$. Figure 3(b) shows the transmission probability through each pathway and interference term obtained with fitted parameters, their summation (yellow dotted line) and raw data (gray solid line) calculated from equation (2). Most of the emission is contributed from pathway I: absorption of two $\hbar\omega$ photons. This can be more clearly revealed by the normalized transmission probability, D_i/D , with i being possible pathways in figure 1(c) or interference terms and D the total transmission probability calculated from equation (2), as shown in figure 3(c). The constructive or destructive interference between those two pathways greatly modulates photoemission. Though not shown, it is found that increasing the intensity ratio between second harmonic to fundamental lasers improves the contribution from pathway II and results in stronger modulation (see figure 5).

Each k -photon ($\hbar\omega$) process (as in equation (2)) also has its photon absorption pathways. The electron emission probability through each k -photon ($\hbar\omega$) process is also a power function of second harmonic laser intensity,

$$w_k^i = C_i (F_2^2)^{(k-s)/2}, \quad (6)$$

where i represents i th pathway, k is the number of total equivalent $\hbar\omega$ photons (as in equation (2)), s is the number of absorbed $\hbar\omega$ photons, $(k-s)/2 = 0, 1, \dots$ is an integer representing the number of absorbed $\hbar(2\omega)$ photons. Interference occurs among different pathways, resulting in high frequency modulation terms. Fourier series coefficients at multiples of second harmonic frequency 2ω for dominant emission channels at $k = 4, 3, 2, 1$, and 0 under the applied DC field of $0, 0.5, 1.5, 3$, and 5 V nm^{-1} respectively are provided in figure A1 in the appendix. They show similar trends and shapes as those in figure 2 for total transmission probabilities. This is reasonable since most of the emission comes from the dominant channel.

Figure 4 shows the transmission probability through k -photon ($\hbar\omega$) processes w_k vs θ , the corresponding Fourier series coefficients and their fittings with quantum pathways interference model, equation (6), and the decomposed results, with $F_0 = 1.5 \text{ V nm}^{-1}$ and $F_1 = 2.6 \text{ V nm}^{-1}$. $k = 2$ is the dominant emission channel under the given fields and contributes to most of the total transmission probability. Therefore, figures 4(a)–(d) share similar trends as those for total transmission probability in figures 2 and 3. When $k = 3$ as shown in figure 4(e), the transmission probability vs θ displays a sinusoidal shape with approximately $\pi/2$ phase delay relative to $w_{k=2}$. Two dominant Fourier coefficients at 0 and 2ω frequencies



are observed in figure 4(f). The summation of components calculated with fitted prefactors overlaps the results calculated from the quantum model. When $k = 4$, three dominant Fourier coefficients are observed at 0 , 2ω , and 4ω frequencies (figure 4(j)). There are three possible pathways as shown in figure 1(a). Their decomposed components and the sum of them agree with those calculated from equation (2).

DC bias field lowers and narrows the cathode surface potential barrier, and therefore shifts the dominant multiphoton process to lower order and alters possible transmission pathways and interference effects among them. The photoemission current is therefore further modulated by DC bias. Figure 5 presents photoemission current modulation depth as a function of DC field and the ratio of F_2 to F_1 with $F_1 = 2.6 \text{ V nm}^{-1}$. When F_2/F_1 is fixed, the modulation depth as a function of F_0 shows two peaks, which has been observed in [43]. The first peak appears at $F_0 = 0$ or 0.5 V nm^{-1} , and the other one is at $F_0 = 2 \text{ V nm}^{-1}$. $F_0 = 0.5 \text{ V nm}^{-1}$ is located at where the transition between four $\hbar\omega$ -photon absorption process ($F_0 = 0$) and three $\hbar\omega$ -photon absorption process occurs. The Schottky barrier lowering by $F_0 = 0.5 \text{ V nm}^{-1}$ is 0.85 eV , resulting in an effective work function of 4.25 eV . The $3 \hbar\omega$ -photon absorption process is above-barrier multiphoton photoemission. It can also be observed that the modulation depth increases to 99.4% at $F_0 = 0.5 \text{ V nm}^{-1}$, $F_1 = 2.6 \text{ V nm}^{-1}$, and $F_2 = 0.25 \text{ V nm}^{-1}$, as indicated by the red pentagram in figure 5, compared to the maximum of 96.8% for $F_0 = 0$, with $F_1 = 2.6 \text{ V nm}^{-1}$ and $F_2 = 0.55 \text{ V nm}^{-1}$. The former has two possible quantum pathways (figure 1(b)) and the interference between them leads to an 2ω frequency term, while the latter has three possible quantum pathways (figure 1(a)) and their interferences lead to both 2ω and 4ω frequency terms [43]. Increase of modulation depth further improves the feasibility of implementing an ultrafast switch with distinct on and off states via electron emission using two-color lasers [14], which is useful in optoelectronics. Furthermore, such an increase of modulation depth does not require any adjustments to the lasers being used, by simply tuning the DC bias [48]. When $1 \leq F_0 \leq 3 \text{ V nm}^{-1}$, the dominant emission process becomes photo-assisted tunneling. $F_0 = 2 \text{ V nm}^{-1}$ is

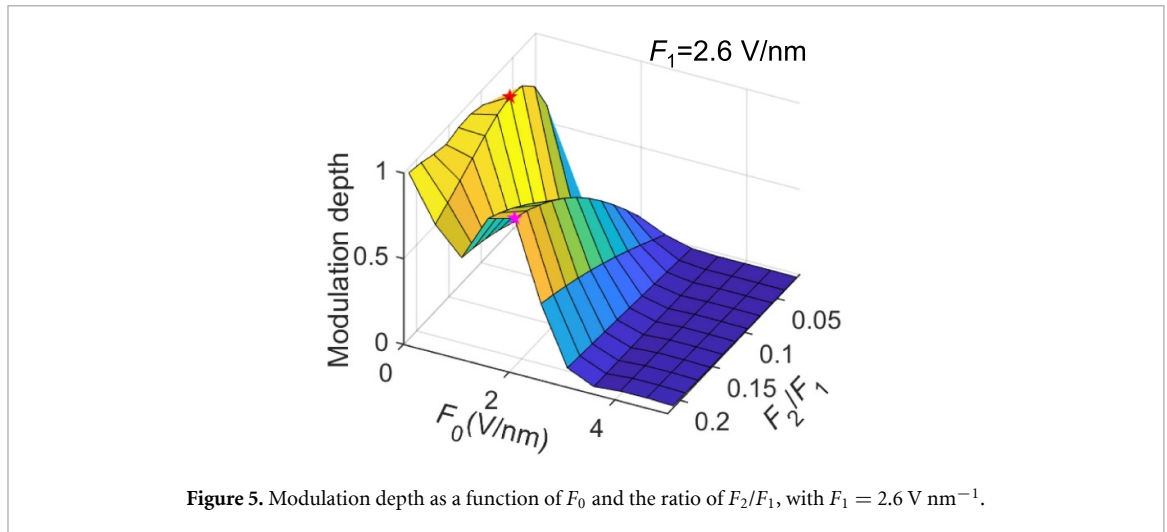


Figure 5. Modulation depth as a function of F_0 and the ratio of F_2/F_1 , with $F_1 = 2.6 \text{ V nm}^{-1}$.

located at where the transition between two and one $\hbar\omega$ -photon assisted tunneling processes occurs. The $2\hbar\omega$ -photon assisted tunneling process has two possible photon absorption pathways (figure 1(c)) and their interference leads to a 2ω frequency term. One $\hbar\omega$ -photon assisted tunneling (figure 1(d)) has only one photon absorption pathway and direct tunneling (figure 1(e)) does not involve photon absorption process. Therefore, modulation of photoemission current becomes weaker as DC bias field increases. When F_0 is fixed and $F_0 \geq 1 \text{ V nm}^{-1}$, it is shown that modulation depth increases with F_2/F_1 . As F_2 increases, photoemission through the dominant k -photon processes under given F_0 and F_1 can be enhanced and the dominant emission channel may shift to a higher order k , which can be found in figure A2 in the appendix. Strong modulation of photoemission can be achieved through tuning the DC field in addition to the two-color laser fields. While relatively small laser fields are considered in the calculations in the current work, it is important to note that strong laser field results in AC Stark shift, which may lead to channel closing and dominant channel shifting to a higher order, and therefore a change in the possible pathways.

3. Conclusion

In conclusion, the effects of DC field on the quantum pathway interference in two-color coherent control of photoemission are analyzed comprehensively using an exact analytical quantum model. The externally applied DC bias lowers and narrows the surface potential barrier, leading to lower order multiphoton absorption photoemission, photo-assisted tunneling and then direct tunneling as DC field increases. The lower order photon absorption processes as aforementioned result in fewer possible pathways and therefore the higher frequency terms (4ω and 2ω) are suppressed sequentially as DC bias field increases. It has been shown that a maximum modulation depth of 99.4% can be achieved when $F_0 = 0.5 \text{ V nm}^{-1}$, $F_1 = 2.6 \text{ V nm}^{-1}$ and $F_2 = 0.25 \text{ V nm}^{-1}$ for a gold emitter with a fundamental laser wavelength of 800 nm. Photoemission under a given set of DC and laser fields includes different k -photon processes. Each k -photon process has its own possible pathways and corresponding interference effects among them. When $k \leq 1$, the interference effects can be negligible. When k increases, there are more possible pathways (single color and multicolor pathways) and interference effects among them. Higher frequency terms and therefore stronger modulation of photoemission can be observed.

It has to be pointed out again here that our quantum model used here involves CW lasers. For laser pulses with a duration much larger than the optical periods ($\text{FWHM} > 10$ cycles), our CW model shows good agreement with both simulations and experiments using pulsed lasers [30, 40] and the relative phase delay between those two lasers (rather than the pulse duration) determines the dynamics of the photoemission. When laser pulses are comparable to or less than 10 cycles, the carrier-envelope phase becomes an important factor that affects the photoemission processes [49, 50]. It is of great interest to study the coherent control of photoemission under ultrashort two-color laser pulses in the future.

Our study reveals the physics behind the effects of DC field on quantum pathways interference in two-color laser induced photoemission. Our results help explain the experimentally observed peaks in curves of modulation depth/visibility vs DC bias and their decreasing trend with DC bias [31]. This systematic analysis of DC effects on quantum pathways using exact analytical solutions of the TDSE provides further insights into enhanced tunability of two-color photoemission using DC bias, and may be helpful in general

coherent control schemes. It is of essential importance to identify and quantify quantum pathways and the corresponding interference effects (magnitude and phase) to understand, design and utilize quantum systems. Our analysis based on exact analytical quantum model enables a comprehensive and explicit examination of the parametric dependence of individual pathways and the interference effects among them. Such a systematic investigation facilitates a better understanding of the parametric scaling of various pathways, thereby aiding in the optimization of input DC and laser parameters to achieve coherent control through a specific pathway in a given quantum system.

Data availability statement

All data that support the findings of this study are included within the article (and any supplementary files).

Acknowledgments

This work was supported by Office of Naval Research (ONR) YIP Grant No. N00014-20-1-2681, and Air Force Office of Scientific Research (AFOSR) Grant Nos. FA9550-20-1-0409 and FA9550-22-1-0523.

Appendix

1. Fourier analysis for the dominant emission process at a given DC field

Figure A1 shows the Fourier series coefficients at multiples of second-harmonic laser frequency 2ω for $w_k(\varepsilon = E_F)$ vs θ with k being the dominant photon absorption process under the given DC field. Since dominant k -photon processes (see figures 1(f)–(j) in main text) contribute to the majority of total emission D , it is clear that Fourier series coefficients share similar trends and values as figure 2 for Fourier series coefficient for D vs θ . When $F_0 = 0$ ($k = 4$), three dominant components at $0, 2\omega, 4\omega$ are observed. As F_0 increases, the dominant channel shifts towards lower k channel. When $F_0 = 0.5$ ($k = 3$) and 1.5 ($k = 2$) V nm^{-1} , two dominant components at 0 and 2ω frequencies are observed. When $F_0 = 3$ ($k = 1$) and 5 ($k = 0$) V nm^{-1} , only zero-frequency term can be observed.

2. Electron transmission probability w_k

Figure A2 shows the electron emission probability from Fermi level $w_k(\varepsilon = E_F)$ through k -photon ($\hbar\omega$) processes under a DC field of $0.5, 1, 1.5, 2, 2.5,$ and 3 V nm^{-1} , with the fundamental laser field $F_1 = 2.6 \text{ V nm}^{-1}$, the second harmonic laser field F_2 being from 0.05 to 0.55 V nm^{-1} , and the relative phase $\theta = 0$. The metal is assumed to be gold, with $W_0 = 5.1 \text{ eV}$ and $E_F = 5.53 \text{ eV}$. The fundamental laser has a wavelength of 800 nm ($\hbar\omega = 1.55 \text{ eV}$). It is observed that increasing the applied DC field shifts the dominant emission process to lower order multiphoton photoemission, photo-assisted tunneling or direct tunneling. The dominant k -photon ($\hbar\omega$) processes are $3, 2, 2, 2, 1$ or 2 (depending on F_2/F_1), and 1 , corresponding to $F_0 = 0.5, 1, 1.5, 2, 2.5,$ and 3 V nm^{-1} in figures A2(a)–(f). When F_2 increases, i.e., F_2/F_1 increases, contribution from higher order k -photon processes becomes larger, which is especially clear for $F_0 = 2.5 \text{ V nm}^{-1}$, as shown in figure A2(e).

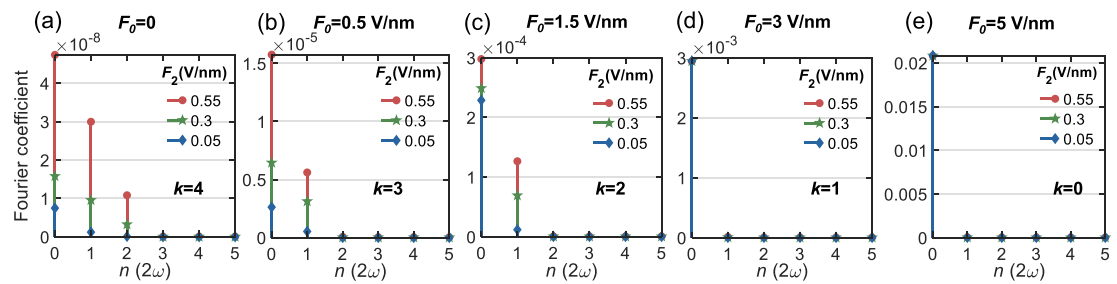


Figure A1. Coefficients of Fourier series expansion for w_k vs θ under a DC field of (a) $F_0 = 0$, with $k = 4$; (b) $F_0 = 0.5 \text{ V nm}^{-1}$, with $k = 3$; (c) $F_0 = 1.5 \text{ V nm}^{-1}$, with $k = 2$; (d) $F_0 = 3 \text{ V nm}^{-1}$, with $k = 1$; and (e) $F_0 = 5 \text{ V nm}^{-1}$, with $k = 0$. Here, $F_1 = 2.6 \text{ V nm}^{-1}$, and $F_2 = 0.05, 0.3, \text{ and } 0.55 \text{ V nm}^{-1}$ for lines in blue, green, and red, respectively.

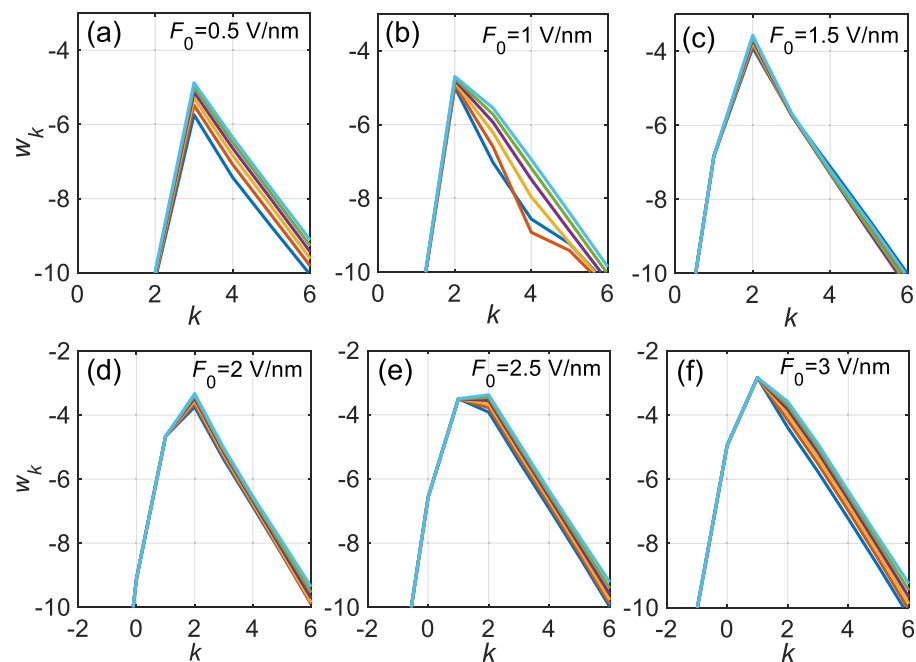


Figure A2. Electron transmission probability from initial energy $\varepsilon = E_F$, $w_k(\varepsilon = E_F)$, through k -photon ($\hbar\omega$) processes, with phase delay $\theta = 0$, $F_1 = 2.6 \text{ V nm}^{-1}$, and $F_2 = 0.05, 0.15, 0.25, 0.35, 0.45, \text{ and } 0.55 \text{ V nm}^{-1}$ corresponding to lines from bottom to top in subfigures.

ORCID iDs

Yang Zhou  <https://orcid.org/0000-0001-6972-4822>

Peng Zhang  <https://orcid.org/0000-0003-0606-6855>

References

- [1] Xie X *et al* 2012 Attosecond probe of valence-electron wave packets by subcycle sculpted laser fields *Phys. Rev. Lett.* **108** 193004
- [2] Gruson V *et al* 2016 Attosecond dynamics through a fano resonance: monitoring the birth of a photoelectron *Science* **354** 734
- [3] Förster M, Paschen T, Krüger M, Lemell C, Wachter G, Libisch F, Madlener T, Burgdörfer J and Hommelhoff P 2016 Two-color coherent control of femtosecond above-threshold photoemission from a tungsten nanotip *Phys. Rev. Lett.* **117** 217601
- [4] Cushing S K 2017 Plasmonic hot carriers skip out in femtoseconds *Nat. Photon.* **11** 748
- [5] Dienstbier P, Seiffert L, Paschen T, Liehl A, Leitenstorfer A, Fennel T and Hommelhoff P 2023 Tracing attosecond electron emission from a nanometric metal tip *Nature* **616** 702
- [6] Brugnara L, Hoffmann D J, Siegel T, Frank F, Zaïr A, Tisch J W G and Marangos J P 2011 Trajectory selection in high harmonic generation by controlling the phase between orthogonal two-color fields *Phys. Rev. Lett.* **107** 153902
- [7] Zhang H, Liu X, Jin F, Zhu M, Yang S, Dong W, Song X and Yang W 2021 Coherent control of high harmonic generation driven by metal nanotip photoemission *Chin. Phys. Lett.* **38** 063201
- [8] Joly A G, El-Khouiry P Z and Hess W P 2018 Spatiotemporal imaging of surface plasmons using two-color photoemission electron microscopy *J. Phys. Chem. C* **122** 20981

- [9] Ji B, Song X, Dou Y, Tao H, Gao X, Hao Z and Lin J 2018 Two-color multiphoton emission for comprehensive reveal of ultrafast plasmonic field distribution *New J. Phys.* **20** 073031
- [10] Zhao Z, Lang P, Qin Y, Ji B, Song X, Song X, Lin J and Lin J 2020 Distinct spatiotemporal imaging of femtosecond surface plasmon polaritons assisted with the opening of the two-color quantum pathway effect *Opt. Express* **28** 19023
- [11] Rybka T, Ludwig M, Schmalz M F, Knittel V, Brida D and Leitenstorfer A 2016 Sub-cycle optical phase control of nanotunnelling in the single-electron regime *Nat. Photon.* **10** 667
- [12] Forati E, Dill T J, Tao A R and Sevenpiper D 2016 Photoemission-based microelectronic devices *Nat. Commun.* **7** 13399
- [13] Zhang P, Valfells Á, Ang L K, Luginsland J W and Lau Y Y 2017 100 years of the physics of diodes *Appl. Phys. Rev.* **4** 011304
- [14] Lang P, Ji B, Song X, Dou Y, Tao H, Gao X, Hao Z and Lin J 2018 Ultrafast switching of photoemission electron through quantum pathways interference in metallic nanostructure *Opt. Lett.* **43** 5721
- [15] Ludwig M, Kazansky A K, Aguirregabiria G, Marinica D C, Falk M, Leitenstorfer A, Brida D, Aizpurua J and Borisov A G 2020 Active control of ultrafast electron dynamics in plasmonic gaps using an applied bias *Phys. Rev. B* **101** 241412
- [16] Xiong X, Zhou Y, Luo Y, Li X, Bosman M, Ang L K, Zhang P and Wu L 2020 Plasmon-enhanced resonant photoemission using atomically thick dielectric coatings *ACS Nano* **14** 8806
- [17] Zhang P, Ang Y S, Garner A L, Valfells Á, Luginsland J W and Ang L K 2021 Space-charge limited current in nanodiodes: ballistic, collisional, and dynamical effects *J. Appl. Phys.* **129** 100902
- [18] Zewail A H 2010 Four-dimensional electron microscopy *Science* **328** 187
- [19] Najafi E, Scarborough T D, Tang J and Zewail A 2015 Four-dimensional imaging of carrier interface dynamics in p-n junctions *Science* **347** 164
- [20] Adhikari A, Eliason J K, Sun J, Bose R, Flannigan D J and Mohammed O F 2017 Four-dimensional ultrafast electron microscopy: insights into an emerging technique *ACS Appl. Mater. Interfaces* **9** 3
- [21] Feist A *et al* 2017 Ultrafast transmission electron microscopy using a laser-driven field emitter: femtosecond resolution with a high coherence electron beam *Ultramicroscopy* **176** 63
- [22] Arbouet A, Caruso G M and Houdellier F 2018 Ultrafast transmission electron microscopy: historical development, instrumentation, and applications *Advances in Imaging and Electron Physics* ed P W Hawkes vol 207 (Elsevier) ch 1, pp 1–72
- [23] Sun S, Sun X, Bartles D, Wozniak E, Williams J, Zhang P and Ruan C-Y 2020 Direct imaging of plasma waves using ultrafast electron microscopy *Struct. Dyn.* **7** 064301
- [24] Graves W S, Kärtner F X, Moncton D E and Piot P 2012 Intense superradiant x-rays from a compact source using a nanocathode array and emittance exchange *Phys. Rev. Lett.* **108** 263904
- [25] Swanwick M E, Keathley P D, Fallahi A, Krogen P R, Laurent G, Moses J, Kärtner F X and Velásquez-García L F 2014 Nanostructured ultrafast silicon-tip optical field-emitter arrays *Nano Lett.* **14** 5035
- [26] Gruse J-N *et al* 2020 Application of compact laser-driven accelerator x-ray sources for industrial imaging *Nucl. Instrum. Methods Phys. Res. A* **983** 164369
- [27] Pellegrini C 2016 X-ray free-electron lasers: from dreams to reality *Phys. Scr.* **2016** 014004
- [28] Seiffert L, Paschen T, Hommelhoff P and Fennel T 2018 High-order above-threshold photoemission from nanotips controlled with two-color laser fields *J. Phys. B: At. Mol. Opt. Phys.* **51** 134001
- [29] Luo Y and Zhang P 2018 Ultrafast strong-field photoelectron emission due to two-color laser fields *Phys. Rev. B* **98** 165442
- [30] Luo Y and Zhang P 2019 Analysis of two-color laser-induced electron emission from a biased metal surface using an exact quantum mechanical solution *Phys. Rev. Appl.* **12** 044056
- [31] Dienstbier P, Paschen T and Hommelhoff P 2021 Two-color coherent control in photoemission from gold needle tips *J. Phys. B: At. Mol. Opt. Phys.* **54** 134002
- [32] Zhou Y 2022 Photoemission from biased metal surfaces: quantum efficiency, laser heating, dielectric coatings, and quantum pathways interference *PhD Thesis* Michigan State University
- [33] Paschen T, Förster M, Krüger M, Lemell C, Wachter G, Libisch F, Madlener T, Burgdörfer J and Hommelhoff P 2017 High visibility in two-color above-threshold photoemission from tungsten nanotips in a coherent control scheme *J. Mod. Opt.* **64** 1054
- [34] Huang W C W, Becker M, Beck J and Batelaan H 2017 Two-color multiphoton emission from nanotips *New J. Phys.* **19** 023011
- [35] Heide C, Boolakee T, Eckstein T and Hommelhoff P 2021 Optical current generation in graphene: CEP control vs. $\omega+2\omega$ control *Nanophotonics* **10** 3701
- [36] Li A, Pan Y, Dienstbier P and Hommelhoff P 2021 Quantum interference visibility spectroscopy in two-color photoemission from tungsten needle tips *Phys. Rev. Lett.* **126** 137403
- [37] Wimmer L, Herink G, Solli D R, Yalunin S V, Echterkamp K E and Ropers C 2014 Terahertz control of nanotip photoemission *Nat. Phys.* **10** 432
- [38] Herink G, Wimmer L and Ropers C 2014 Field emission at terahertz frequencies: AC-tunneling and ultrafast carrier dynamics *New J. Phys.* **16** 123005
- [39] Wimmer L, Karnbach O, Herink G and Ropers C 2017 Phase space manipulation of free-electron pulses from metal nanotips using combined terahertz near fields and external biasing *Phys. Rev. B* **13** 165416
- [40] Zhang P and Lau Y Y 2016 Ultrafast strong-field photoelectron emission from biased metal surfaces: exact solution to time-dependent schrödinger equation *Sci. Rep.* **6** 19894
- [41] Zhou Y and Zhang P 2020 A quantum model for photoemission from metal surfaces and its comparison with the three-step model and fowler-dubridge model *J. Appl. Phys.* **127** 164903
- [42] Zhou Y and Zhang P 2021 Quantum efficiency of photoemission from biased metal surfaces with laser wavelengths from UV to NIR *J. Appl. Phys.* **130** 064902
- [43] Zhou Y and Zhang P 2022 Unraveling quantum pathways interference in two-color coherent control of photoemission with bias voltages *Phys. Rev. B* **106** 085402
- [44] Papadogiannis N A, Moustazis S D and Girardeau-Montaut J P 1997 Electron relaxation phenomena on a copper surface via nonlinear ultrashort single-photon photoelectric emission *J. Phys. D: Appl. Phys.* **30** 2389
- [45] Ropers C, Solli D R, Schulz C P, Lienau C and Elsaesser T 2007 Localized multiphoton emission of femtosecond electron pulses from metal nanotips *Phys. Rev. Lett.* **98** 043907
- [46] Kildemo M, Calatroni S and Taborelli M 2004 Breakdown and field emission conditioning of Cu, Mo, and W *Phys. Rev. Accel. Beams* **7** 092003
- [47] Yoshioka K, Katayama I, Minami Y, Kitajima M, Yoshida S, Shigekawa H and Takeda J 2016 Real-space coherent manipulation of electrons in a single tunnel junction by single-cycle terahertz electric fields *Nat. Photon.* **10** 762

- [48] Turchetti M, Bionta M R, Yang Y, Ritzkowski F, Ritzkowski F, Candido D R, Flatté M E, Berggren K K and Keathley P D 2021 Impact of DC bias on weak optical-field-driven electron emission in nano-vacuum-gap detectors *J. Opt. Soc. Am. B* **38** 1009
- [49] Keathley P D, Putnam W P, Vasireddy P, Hobbs R G, Yang Y, Berggren K K and Kärtner F X 2019 Vanishing carrier-envelope-phase-sensitive response in optical-field photoemission from plasmonic nanoantennas *Nat. Phys.* **15** 1128
- [50] Luo Y, Zhou Y and Zhang P 2021 Few-cycle optical-field-induced photoemission from biased surfaces: an exact quantum theory *Phys. Rev. B* **103** 085410